frontiers | Frontiers in Built Environment

TYPE Original Research
PUBLISHED 12 December 2022
DOI 10.3389/fbuil.2022.1083266

OPEN ACCESS

EDITED BY
Dario De Domenico,
University of Messina, Italy

REVIEWED BY
Emanuele Gandelli,
University of Brescia, Italy
Marco Furinghetti,
University of Pavia, Italy
Zhipeng Zhao,
Tohoku University, Japan

*CORRESPONDENCE
Antonio Di Cesare,
antonio.dicesare@unibas.it

SPECIALTY SECTION
This article was submitted to Earthquake Engineering,
a section of the journal
Frontiers in Built Environment

RECEIVED 28 October 2022
ACCEPTED 10 November 2022
PUBLISHED 12 December 2022

CITATION
Di Cesare A, Ponzo FC and Telesca A (2022), Mechanical model of the over-stroke displacement behaviour for double concave surface slider anti-seismic devices.
Front. Built Environ. 8:1083266.
doi: 10.3389/fbuil.2022.1083266

Mechanical model of the over-stroke displacement behaviour for double concave surface slider anti-seismic devices

Antonio Di Cesare*, Felice Carlo Ponzo and Alessio Telesca

School of Engineering, University of Basilicata, Potenza, Italy

For double concave curved surface slider (DCCSS) isolators with a flat rim and lacking restrainers, such as those most commonly used in Europe, the rigid slider can exceed the geometrical capability of the housing plate during earthquakes stronger than those produced in simulations. During this over-stroke displacement, DCCSSs preserve the ability to support superstructure gravity loads and the capacity to dissipate energy. There are currently no applicable hysteresis rules or available algebraic solutions that can be used to predict over-stroke behaviour for response-history analysis. This study presents an algebraic solution to extend basic theories for estimating the actual limit displacement of DCCSS devices with over-stroke capacity. DCCSS behaviour in the over-stroke sliding regime was modelled with a focus on geometrical compatibility and kinematics. The proposed analytical formulation was calibrated on the basis of experimental controlled-displacement tests performed on single DCCSS devices. A case study of a six-storey reinforced concrete frame isolated building was modelled using a combination of non-linear elements that are currently available in several structural analysis software packages and able to correctly model over-stroke displacement behaviour for non-linear time history analyses. The DCCSS model was augmented with a friction model capable of accounting for torsional effects, axial load, and velocity variabilities. Comparison with non-linear dynamic analysis outcomes shows that the forces and displacements in the over-stroke sliding regime are predictable and therefore useful for the designer.

KEYWORDS

base isolation, double concave curved surface slider, over-stroke displacement, mechanical modelling, experimental tests, non-linear dynamic analysis

1 Introduction

Isolation devices are designed to uncouple the movement of the structure from the underlying ground, and this attribute is granted by their low horizontal stiffness. The most commonly used isolation devices are elastomeric and sliding bearings, such as curved surface sliders (CSSs) (Zayas et al., 1987), which are being increasingly used in the seismic isolation systems of buildings and bridges.

Double concave curved surface slider (DCCSS) isolation bearings consist of two facing concave stainless-steel surfaces separated by an inner rigid slider characterized by Φ_s diameter and h_s height (as shown in Figure 1A). The forces acting on the slider (see Figure 1B) are the vertical load W, the resultant forces of normal pressure acting on the sliding interfaces N, the lateral force F, and the friction force S, acting along the curved surfaces (Mostaghel and Davis, 1997). The radius of curvature and the friction coefficient are the main key parameters. Compared with traditional CSSs, the main advantage of DCCSS bearings is their lower cost due to their more compact size.

Previous studies have proposed a variety of numerical modelling and experimental tests for slider isolators (Constantinou et al., 1990; Almazán and De La LLera 1998, 2011; Fenz and Constantinou 2006; Fenz and Constantinou 2008a; 2008b; Becker and Mahin 2012a; 2012b; Lomiento et al., 2013; Sarlis and Constantinou 2016; Ponzo et al., 2017, 2019, 2020, 2021; De Domenico et al., 2018, 2019; Pavese et al., 2018; Di Cesare et al., 2019, 2021; Pigouni et al., 2019; Quaglini et al., 2012, 2019; Furinghetti et al., 2020) that also involve geometrical compatibility and multibody kinematics formulations (Belfiore et al., 2000; Shabana 2001; Tsai et al., 2005; Popov 2010; Mazza et al., 2017; Nikravesh 2018; Bianco et al., 2020, 2021). Additionally, the behaviour of single and multiple concave surface sliding bearings has been analytically characterized by Sarlis Constantinou (2013).

The analytical description of the DCCSS bearings characterized by the same radii of curvature $R_1 = R_2 = R$ and same coefficients of friction $\mu_1 = \mu_2 = \mu$ is shown below. Angles ϑ_i are formed by the lines connecting the centre of curvature of the concave plates ("1" for the bottom concave plate [BCP] and "2" for the top concave plate [TCP]) and the central point of the contact area between slider and plate, while angles $\vartheta_{s,i}$ form between the latter of these points and the points of application of the resultant forces at the surface of the slider. Angles are considered to be small so that the normal components of force are equal to the applied load W (see Figure 1B).

$$\vartheta_1 = \frac{\mathbf{d}}{(\mathbf{R_1} - \mathbf{h_s})} \tag{1}$$

Imposing the constraint of TCP being horizontal during motion, the angles can be represented as:

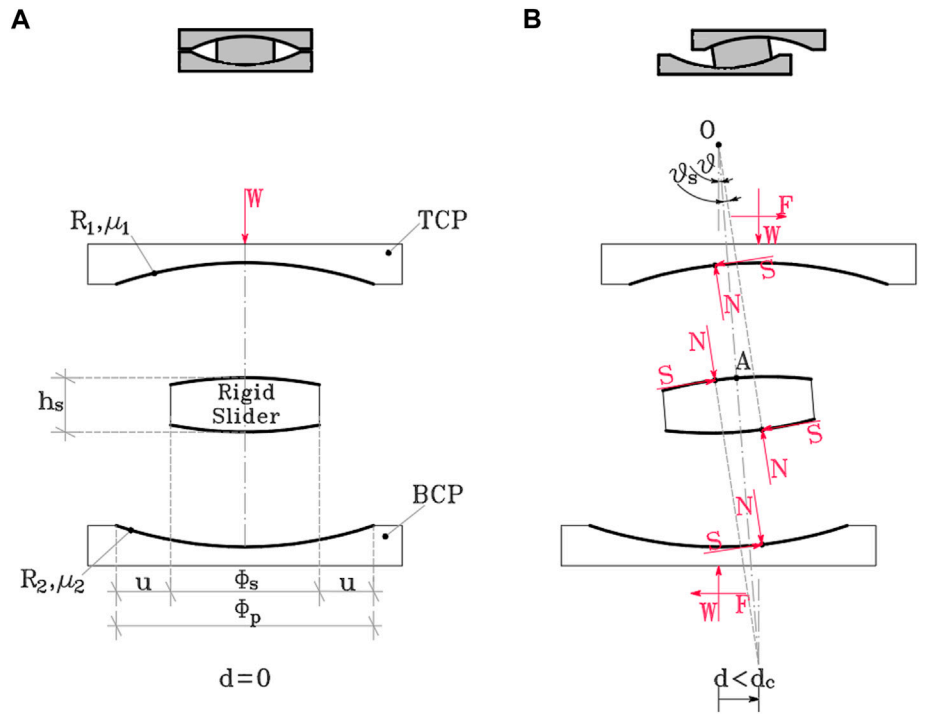

FIGURE 1
Exploded cross-section of the DCCSS bearing. in static conditions **(A)** and in the sliding regime **(B)** (Sarlis and Constantinou 2013).

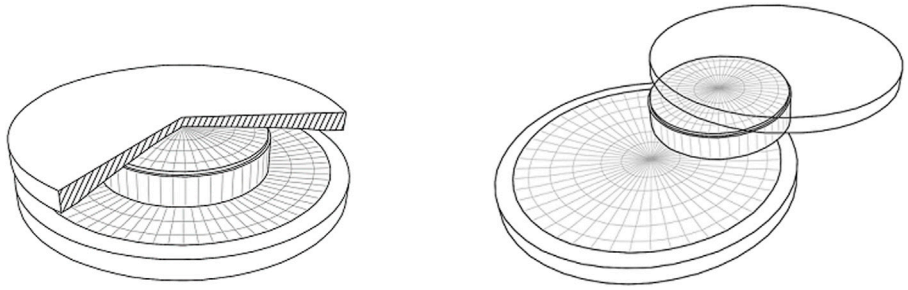

FIGURE 2
Perspective view of the DCCSS in the static condition and in the over-stroke regime.

$$\vartheta_{s1} = \vartheta_{s2} = \vartheta_s \quad (2)$$

$$\vartheta_1 = \vartheta_2 = \vartheta \quad (3)$$

The resultant force N must be eccentric to satisfy moment equilibrium; accordingly, the pressure distribution on the sliding interface is not uniform. The equilibrium of moments for the slider around A (Eq. 4a) and (3horizontal) equilibrium of forces for the TCP (Eq. 4b) are as follows:

$$\begin{cases} \mathbf{W}(\vartheta_s \mathbf{R} + \vartheta_s \mathbf{R}) - \mathbf{W}\vartheta_s \mathbf{h_s} - \mathbf{S}\mathbf{h_s} = \mathbf{0}\ (a) \\ \mathbf{W}(\vartheta + \vartheta_s) + \mathbf{S} = \mathbf{F}\ (b) \end{cases} \quad (4)$$

From Eq. 4 and (3the) value of angle ϑ_s can be expressed as follows:

$$\vartheta_s = \frac{\mu \mathbf{h_s}}{\mathbf{R_{eff}}} \quad (5)$$

Substituting Eq. 5 into Eq. 4 results in the following:

$$\mathbf{F} = \mu \mathbf{W}\left(1 + \frac{\mu \mathbf{h_s}}{\mathbf{R_{eff}}}\right) + \mathbf{W}\vartheta \quad (6)$$

Considering that the displacement of the TCP is given by $d = (R - h_s)\vartheta + R\vartheta$ and that $R_{eff} = R_1 + R_2 - h_s = 2R - h_s$, when substituting this into Eq. 6, the force-displacement relationship of the bearing is:

$$\mathbf{F} = \mathbf{W}\left(2\frac{\mu \mathbf{R}}{\mathbf{R_{eff}}}\right) + \mathbf{W}\frac{\mathbf{d}}{\mathbf{R_{eff}}} \quad (7)$$

Further details about this equation can be found in Sarlis and Constantinou (2013, Sarlis and Constantinou (2016).

During ground motions with intensities higher than those in simulations, the rigid slider in DCCSSs with flat rims and lacking elements can shift beyond the geometrical capacity of the housing plates in the so-called over-stroke regime (see Figure 2). Over-stroke displacement capacity is a crucial element that can reduce the annual frequency of the collapse displacement being exceed and improve the seismic resilience of a structure that is isolated with these bearings (Di Cesare et al., 2021). However, the mechanical description of this phenomenon has yet to be explored. This paper focuses on the development of an analytical model, based on fundamental mechanical principles, to describe the over-stroke behaviour of DCCSS devices and define their actual limit displacement.

Following a report by Bao et al. (2017), the envisioned mode of behaviour in the over-stroke regime and the corresponding multi-body kinematic were calibrated in *ad hoc* experimental tests conducted on devices pushing the horizontal displacement beyond geometrical capability, revealing how the displacement limit better preserves the ability to support vertical loads (Furinghetti et al., 2021a; Di Cesare et al., 2021). The objective of this was to propose an easy tool for predicting limit displacement and the corresponding shear force, starting from the geometrical and mechanical characteristics of the devices.

The proposed formulation was applied in a case study of a six-storey RC-frame-isolated building. A multi-degree of freedom (MDoF) model was implemented for non-linear dynamic analyses that considered three sets of 20 horizontal earthquakes characterized by intensity values around the collapse limit state (CLS) design spectrum. The comparison between the non-linear numerical results accounting for the friction dependencies from variability in the dynamic condition of velocity and axial load, and the proposed algebraic solution defined in the static condition, accurately predicted of over-stroke force and displacement.

2 Mechanical model of over-stroke displacement

In the case of DCCSS bearings with a flat rim without restraining elements, the limit displacement d_{lim} was able to correspond to the slider overturning around its centre of rotation (d_{ot} displacement) beyond the geometrical capacity $d_C = 2u$ if failure for maximum contact pressure was avoided (d_p displacement) (see Figure 3, Figure 4B).

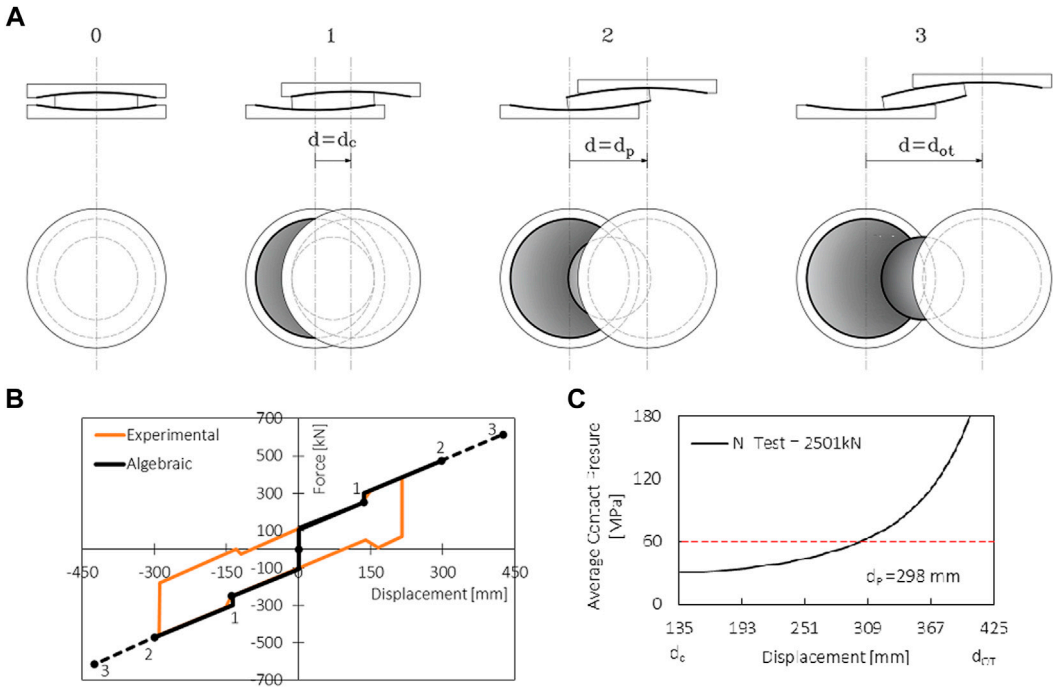

FIGURE 3
(A) Cross-sections and planar views of the DCCSS test specimen (Di Cesare et al., 2019) in three main deformed stages. **(B,C)** Test diagrams of force **(B)** and average contact pressure vs. displacement **(C)**.

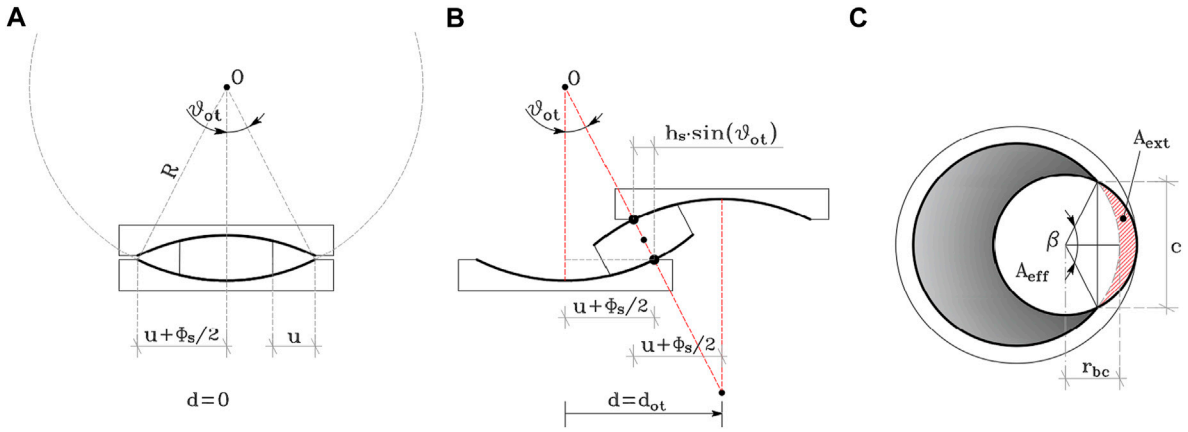

FIGURE 4
Cross-section of the DCCSS in: **(A)** static conditions **(A)** and the over-stroke regime **(B)**. **(C)** Planar view of the rigid slider and the housing plate in the over-stroke regime.

The assumptions of this study were that the bottom and top concave plates are characterized by the same radii of curvature and the same coefficients of friction ($R_1 = R_2$ and $\mu_1 = \mu_2$), and the outcome is that the sliding occurs simultaneously on both surfaces. Two main sliding regimes were considered for horizontal displacement d, which were as follows:

-within the geometric capacity (Regime I): $0 < |d| < d_c$, see Eq. 7

TABLE 1 Main characteristics of the DCCSS specimen and the over-stroke experimental test.

	Sliding regime					Over-stroke regime			
	W	R_{eff}	μ	Φ_s	d_c	$\Delta\mu$	d_p	d_{ot}	F_{lim}
	[kN]	[mm]	[-]	[mm]	[mm]	[-]	[mm]	[mm]	[kN]
Experimental	2,500	2,500	0.04	310	±136	0.015	±298	±425	474.34

-in the over-stroke condition (Regime II): $d_c \leq |d| \leq d_{lim} = min\left\{d_{ot}; d_p\right\}$

The maximum shear force developed by the device and transferred from the superstructure to the foundation was defined as force $F_{lim} = F(d_{lim})$ at the limit displacement d_{lim} (see Eq. 8).

Controlled displacement tests on DCCSS bearings were performed to investigate the actual response of the device when the sliding displacement exceeds the displacement capacity and runs over the sliding surfaces (Di Cesare et al., 2019; Ponzo et al., 2020). The main characteristics of the DCCSS specimen and the experimental testing results are summarized in Table 1 (Di Cesare et al., 2021). The testing protocol consisted of one cycle at constant velocity $v = 2.5\,mm/sec$ and constant vertical load W (Table 1), performed with a 'triangular-shaped' controlled displacement. The maximum displacement reached during the test d_{exp} was more than two times the geometric capacity displacement d_c ($d_{exp}/d_c \approx 2.1$).

Experimental results showed that when the rigid slider overcomes the concave sliding surface edge (position 1, Figure 3A), it can move up to half of its diameter (position 3, Figure 3A), resulting in a slight increase in force (black line in Figure 3B). In the loading and unloading phases of the first cycle, DCCSS over-stroke behaviour was characterized by a 'sloping dog bone' shape, preserving re-centring capability and the ability to support the gravity load. A sudden increase in horizontal force and local equivalent stiffness occured as the sliding pad travelled beyond the housing plate edge (Figure 3C). From a mechanics point of view, this behaviour may have occurred due to an increase in the friction coefficient $\Delta\mu = 0.015$ as the sliding pad came into contact with the small edge of the housing plate sliding material (counterbore gap material). The test was stopped at displacement d_p when the maximum contact pressure of the sliding material was reached (Figure 3C); polytetrafluoroethylene (PTFE)-based sliding material with an allowable contact pressure of $\sigma_a = 60$ MPa was assumed based on experimental observations. Only a small amount of degradation of the inner slider PTFE surfaces, and zero isolator damage, were observed after one cycle of sliding above the edge of the device.

In the over-stroke stage of motion (Regime II), the previously exposed Eq. 7 could be properly modified to take an increased friction coefficient $\mu_2 = \mu + \Delta\mu$ into account, as follows:

$$\mathbf{F} = \mathbf{W}\left(2\frac{\mu_2 \mathbf{R}}{\mathbf{R_{eff}}}\right) + \mathbf{W}\frac{\mathbf{d}}{\mathbf{R_{eff}}} \tag{8}$$

Theoretically, in the over-stroke regime, the failure mechanism linked to the bearing kinematics occurs when overturning displacement d_{ot} is reached (position 3 in Figure 3A, and black dashed line in Figure 3B). Referring to Figure 4 the d_{ot} is identified as the displacement corresponding to the alignment of the TCP and the BCP opposite housing plate edges with the centre of rotation of the slider, and with the centres of curvature of both plates (Figure 4B), defined by the overturning angle ϑ_{ot} and expressed as follows:

$$\boldsymbol{\vartheta_{ot}} = \mathbf{arcsin}\left(\left(\mathbf{u} + \frac{\boldsymbol{\Phi_s}}{2}\right)\Big/\mathbf{R}\right) \tag{9}$$

$$\mathbf{d_{ot}} = \mathbf{2u} + \boldsymbol{\Phi_s} - \mathbf{h_s} \cdot \mathbf{sin}\ (\boldsymbol{\vartheta_{ot}}) \tag{10}$$

Then, if geometric capacity displacement $d_c = 2u$ and Eq. 9 are substituted into Eq. 10, the final expression for the overturning displacement can be written as follows:

$$\boldsymbol{d_{ot}} = \frac{\mathbf{R_{eff}}}{\mathbf{2R}}\left(\boldsymbol{d_c} + \boldsymbol{\Phi_s}\right) \tag{11}$$

It should be noted that the overturning displacement is often not implemented as a failure condition for DCCSSs because the failure of maximum contact pressure on the reduced slider area occurs for a generally shorter displacement $d_p < d_{ot}$.

Regime	Description	Equation	Domain
I	General sliding condition on concave surfaces	$F = \mu W 2\,R/R_{eff} + Wd/R_{eff}$	$0 < \|d\| \leq d_c$
II	Sliding in the over-stroke regime	$F = \mu_2 W 2\,R/R_{eff} + Wd/R_{eff}$	$d_c < \|d\| \leq d_{lim}$
			$d_{lim} = min\left\{d_{ot}; d_p\right\}$

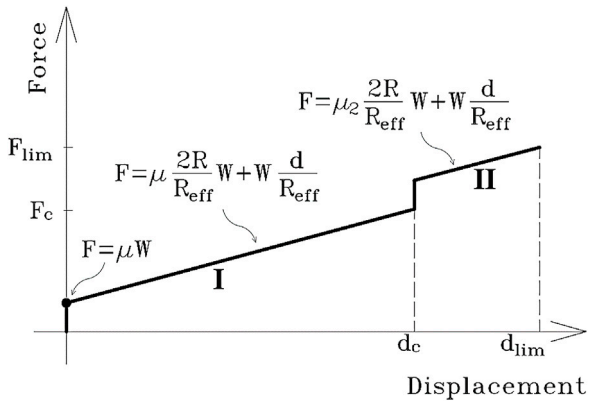

FIGURE 5
Force-displacement backbone curve for the over-stroke behaviour of the DCCSS bearing.

Displacement d_p, associated with the attainment of the limit contact $\sigma_a = W/A_{eff}$ on the sliding interface between the rigid slider and concave plate, is shown in the scheme of Figure 4C. A_{eff} is the effective contact area between the slider and housing plate, and is equal to the slider surface reduced by the area of the slider external to the sliding A_{ext} A_{ext}, as follows:

$$\mathbf{A_{eff}} = \pi\left(\frac{\Phi_s}{2}\right)^2 - \mathbf{A_{ext}} \tag{12}$$

The external area A_{ext} formulation, using simple geometric considerations, is:

$$\mathbf{A_{ext}} = \frac{1}{2}\left(\frac{\Phi_s}{2}\right)^2 \beta - \left(c \cdot \frac{r_{bc}}{2}\right) \tag{13}$$

where β is the angle described by the connection of the intersection point between the slider and the sliding pad circumferences, c is the circumference chord that connects these intersection points, and r_{bc} is the distance between the sliding pad border and the slider centre (see Figure 4C), represented as follows:

$$\beta = 2*\arcsin\left(\frac{c/2}{\Phi_s/2}\right) \tag{14}$$

$$c = 2\sqrt{\left(\frac{\Phi_s}{2}\right)^2 - (r_{bc})^2} \tag{15}$$

$$r_{bc} = d_c + \frac{\Phi_s}{2} - d_p \tag{16}$$

Substituting Eqs 12–15 into Eq. 16, the displacement $d_p = d(\sigma = \sigma_a)$ associated with the limit contact pressure is expressed as:

$$d_p = \frac{2W}{c\,\sigma_a} - \frac{2}{c}\left(\frac{\Phi_s}{2}\right)^2\left(\pi - \arcsin\left(\frac{c}{\Phi_s}\right)\right) + \left(\frac{\Phi_s}{2} + d_c\right) \tag{17}$$

The proposed analytical formulations for sliding in the over-stroke regime (Regime II) is reported below, together with the basic formulation for general sliding conditions (Regime I), as set out by (Sarlis and Constantinou., 2013; Sarlis and Constantinou., 2016).

The backbone curve of the force-displacement relationship is shown in Figure 5. Compared with another recent study (Furinghetti et al., 2021b), the analytical formulation of the over-stroke stage of motion and the definition of the domain of application (Eqs 8, 17) are novel to this study.

The proposed formulation has been compared with a few over-stroke tests described by Furinghetti et al. (2021b) in which a DCCSS specimen characterized by an effective radius of curvature of $R_{eff} = 3080mm$, a slider diameter of $\Phi_s = 260mm$, and a geometric capacity displacement of $d_c = \pm 275mm$ was tested under constant velocity $v = 2.5\,mm/sec$ and constant vertical load W, which were applied to the test apparatus, as shown in Figure 6. Tested DCCSSs were characterized by three different sliding materials: graded polytetrafluoroethylene (PTFE) filled with carbon fibres ($\mu = 0.05$) Figure 6A); ultra low-density polyethylene ($\mu = 0.03$) Figure 6B); and virgin PTFE ($\mu = 0.01$) Figure 6C). The sliding materials implemented into the adopted device have been tested at an average contact pressure of $\sigma = 45\,MPa$ (Furinghetti et al., 2021a). The ratio between the maximum displacement reached during the tests

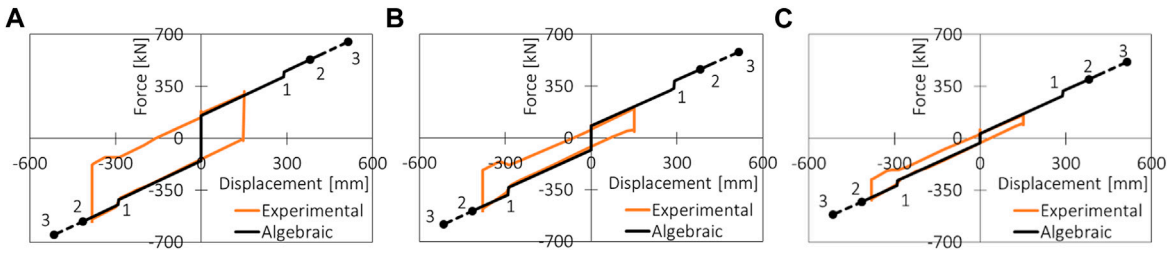

FIGURE 6
Force displacement test results from Furinghetti et al. (2021a) compared with the proposed analytical model for friction values: **(A)** 0.05; **(B)** 0.03; **(C)** 0.01.

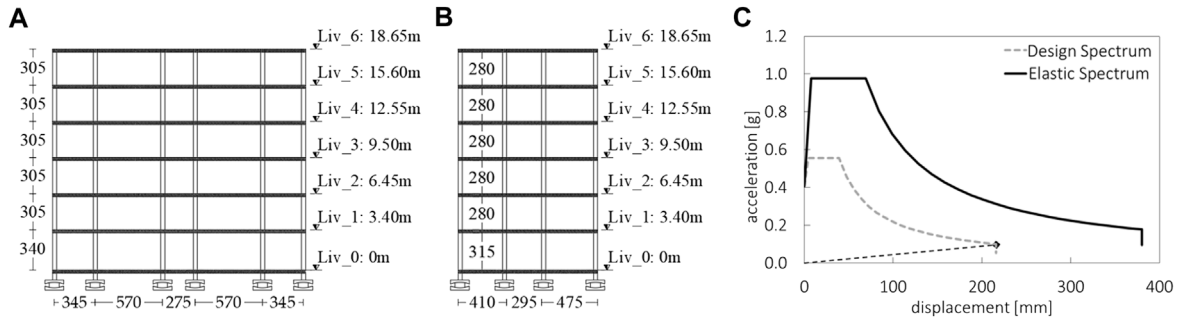

FIGURE 7
(A, B) Longitudinal **(A)** and transversal **(B)** sections of the case study. **(C)** ADRS design spectrum.

TABLE 2 Main characteristics of the DCCSS for the case study.

	Sliding regime								Over-stroke regime			
	W	R_{eff}	μ	Φ_s	T_{eq}	ξ_{eq}	d_{bd}	d_c	$\Delta\mu$	d_p	d_{ot}	F_{lim}
Numerical	[kN]	[mm]	[-]	[mm]	[sec]	[%]	[mm]	[mm]	[-]	[mm]	[mm]	[kN]
	1,133	3,700	0.05	200	2.58	26	216	±330	0.015	420	516	189.68

and the geometric capacity displacement was $d_{exp}/d_c \approx 1.5$. The experimental results showed that in the over-stroke regime, the friction coefficient increases by $\mu = 0.015$ for all tests. Experimental force-displacement results have been replicated using the proposed formulation Figure, which shows that the analytical model is capable of representing DCCSS behaviour during tests with a significantly good approximation. For the experimental cases, the limit displacement can be calculated using the proposed formulation $d_{\lim} = min\{d_{ot} = 515\,mm;\ d_p = 415\,mm\}$. For the sake of safety, in these experimental tests, the isolators were excited at maximum displacements less than d_{lim}, as predicted by analysis. It is worth noting that the experimental tests (Furinghetti et al., 2021a; Di Cesare et al., 2021) were performed assuming a low velocity and constant axial force, so the dependency of the extra-stroke parameters on higher sliding velocities and different contact pressure values still needs to be investigated.

3 Case study

A case study prototype structure was selected for the application of the proposed analytical model. The case study is representative of an existing building, designed according to the outdated İtalian seismic code (Decreto Ministreriale, 1986), with a low seismic design approach, retrofitted using the seismic isolation technique. The building, which is located in the city of L'Aquila (Iervolino et al., 2019), has a regular plan of approximately 240 m^2 square meters and is characterized by a six-storey reinforced concrete (RC) frame structure (see Figure 7,B). The ground level height is 3.4 m, whereas all the other stories are 3.05 m in height. A staircase designed with knee beams is included, and slab thickness is 25 cm for all stories. Infill panels were considered to be regularly distributed in plan and elevation, with different opening percentages.

An isolation system composed of DCCSS bearings was designed for the collapse limit state (CLS), following the Italian seismic code (NTC 2018). The equivalent parameters are summarized in Table 2, where T_{eq} is the equivalent period of the isolated building, ξ_{eq} is the equivalent damping, and d_{bd} is the design displacement (Ponzo et al., 2021). Once the isolation system was designed, the geometrical and mechanical parameters of the isolator shown in Figure 9 were used in the proposed algebraic solution to define displacements d_p and d_{ot}, limit displacement d_{lim}, and the shear force limit F_{lim}. Results are shown in Table 2 and the force-displacement law is shown in Figure 9.

Non-linear time history analyses were carried out to consider 20 different earthquakes (EQ) per three intensity measure levels characterized by return periods T_R of: 500y corresponding to the life safety limit state (LLS); 1000y corresponding to the CLS; and a highest return period of 2500 years from the current Italian seismic code (NTC 2018). Figure 8 shows the elastic spectra of the 20 selected earthquakes for each return period for the main

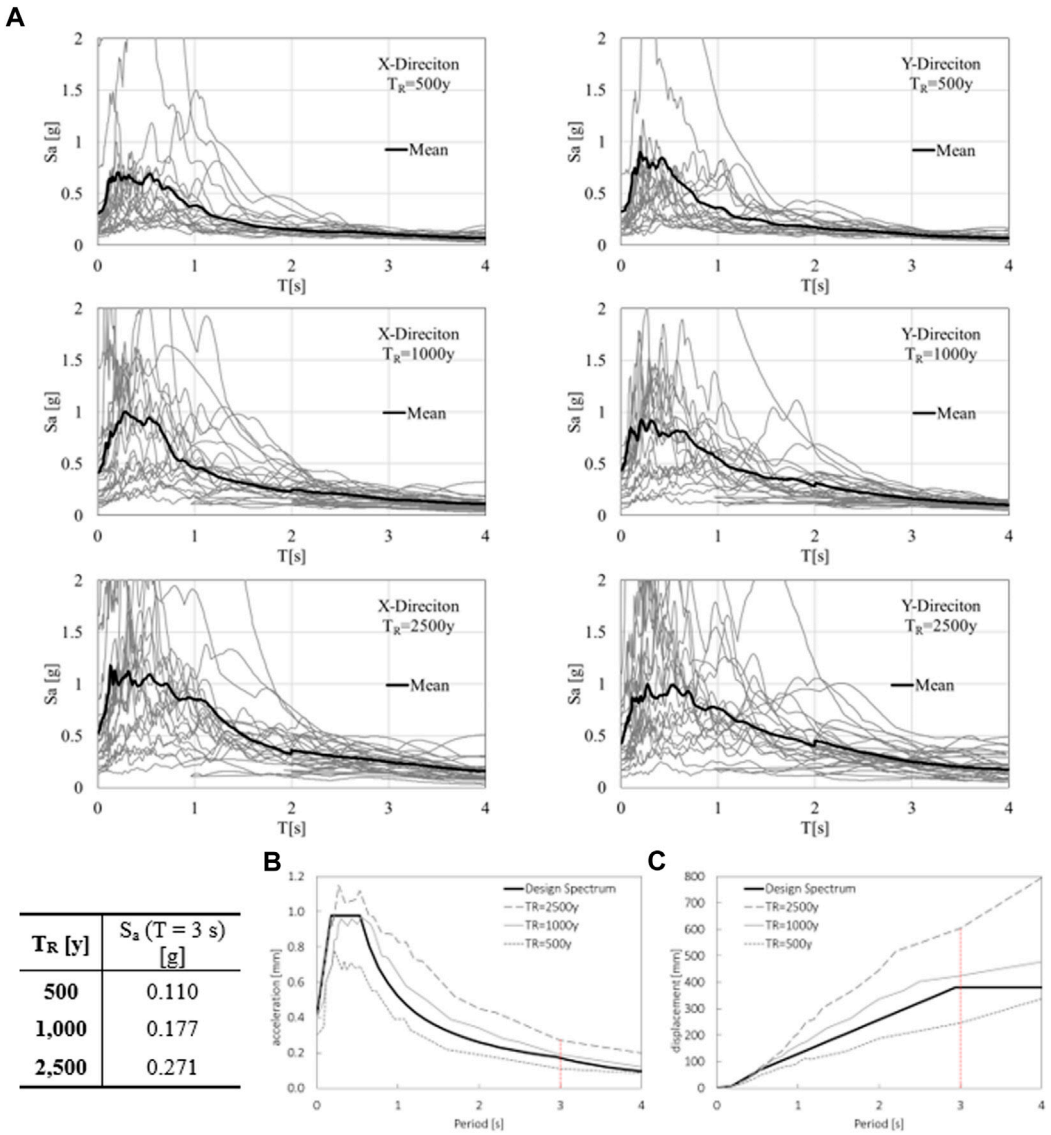

T_R [y]	S_a (T = 3 s) [g]
500	0.110
1,000	0.177
2,500	0.271

FIGURE 8
(A) Acceleration spectra for the 20 chosen records in *X* and *Y* directions for the selected return Periods T_R. **(B, C)** Mean spectral accelerations S_a (T = 3*s*) for the selected return periods T_R, and design and mean spectra of the seismic inputs acceleration **(B)** and displacement **(C)**.

directions (X and Y), and the mean spectrum. All records were selected using spectrum-compatibility criteria, with a fundamental period $T = 3.0\,sec$. Detailed information about the ground motion selection is provided by (Iervolino et al., 2011, Iervolino et al., 2018).

The comparison between the mean spectra at the different return period and the design spectrum is shown in Figure 8B and Figure 8C in terms of pseudo-acceleration and pseudo-displacement. Figure 8 also shows, for each return period, the mean value of the spectral acceleration Sa(T) corresponding to a vibration period of $T = 3.0\,sec$ due to record-to-record variability. Figure 8 highlights how the selected earthquakes cover a wide range of spectral acceleration (Figure 8) and displacements (Figure 8) around the design spectrum.

3.1 Numerical model

A numerical simulation of the isolated building case study has been carried out using OpenSEES software (Mckenna et al., 2000) through non-linear dynamic analyses on a three-dimensional MdoF model.

For MDoF modelling (see Figure 9), the original fixed-based building model was upgraded by introducing a rigid grid at the

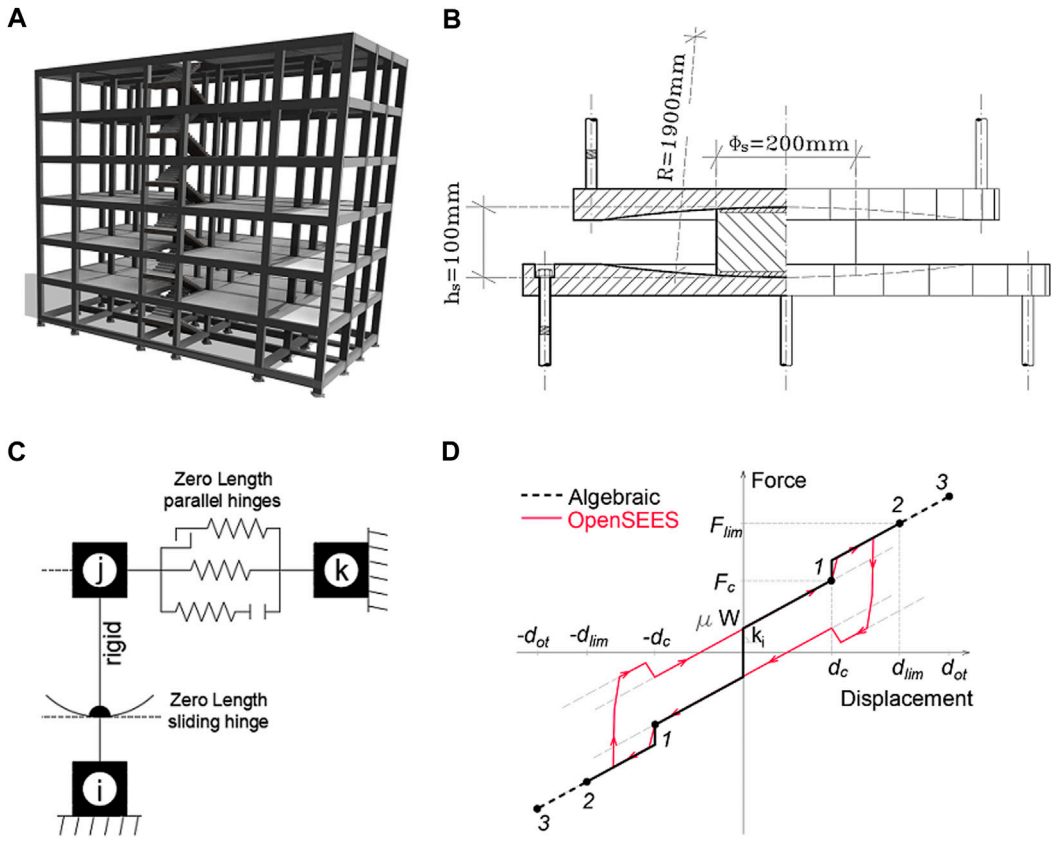

FIGURE 9
(A,B) Proposed case study structure **(A)** and DCCSS isolator **(B)**. **(C)** Representation of the isolator numerical model. **(D)** Sloping dog bone shape constitutive law.

base floor and seismic isolation devices below each column. The superstructure was modelled as a lumped plasticity model implemented at the end of beams and column elements. The flexural behaviour of the plastic hinges was modelled to take axial load interaction effects into account (Ibarra et al., 2005). The model included staircase knee beams and cantilever steps modelled as non-linear elements. A modified version of the model defined by Decanini et al. (2014) was used for masonry infill panels modelled with an equivalent compression-only strut taking into consideration a proper reduction of strength and lateral stiffness due to the influence of openings and potential premature out-of-plane collapse. In this study, 5% Rayleigh damping was used to model the viscous damping of the superstructure as a traditional reinforced concrete fixed-base building. More details regarding the superstructure modelling are provided by Ricci et al. (2018).

To describe the over-stroke behaviour of the DCCSS bearing, the *SingleFPBearing* element (Mckenna et al., 2000), providing a fixed bottom node (i-node) and a top node (j-node), was modified by adding three zero-length parallel hinges between the j-node and an external fixed node (k-node in Figure 9), as already discussed in other studies (Di Cesare et al., 2019, 2021; Ponzo et al., 2020; Ponzo et al., 2021; Cardone et al., 2022). In Figure 9 the resulting sloping dog bone shape for the constitutive law is shown with the main characterizing parameters, such as capacity displacement d_c and force F_c. The simple parallel hinges model composed of non-linear elements was used so that it could be immediately implemented in currently available structural analysis software. The DCCSS model has been provided with a *VelNormalFrcDep* friction model capable of accounting for torsional effects, axial load, and sliding velocity variabilities.

3.2 Summary of results

Figure 10 shows the comparison between the proposed algebraic solution (see Eq 8, 17) and results of non-linear dynamic analyses for records that reached the limit displacement d_{lim}. It is worth noting that for all of the seismic

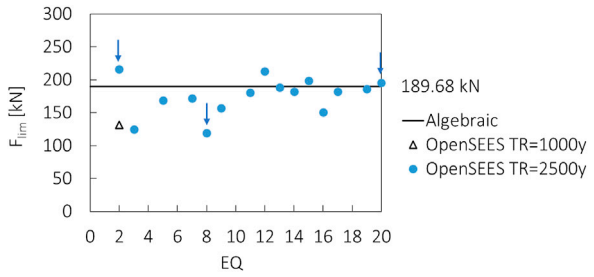

FIGURE 10
Isolation bearing limit shear forces F_{lim} from non-linear analysis compared with the algebraic solution.

intensities, 16 cases out of 60 reached the limit displacement d_{lim}. In particular, for cases with a return period of $T_R = 500y$, all records showed a maximum displacement lower than the capacity displacement d_c of the devices. For $T_R = 1000y$ cases, four records out of 20 reached the capacity displacement d_c, one of which also reached the limit displacement d_{lim}. For high seismic intensity cases $T_R = 2500y$, the displacement d_c was exceeded by 17 records, while d_{lim} was exceeded by 15, as shown in Figure 10.

The F_{lim} value can be considered as the maximum shear force acting on the DCCSS; it is useful to properly design the device and its connections to the structure and the foundation. These connections are designed to transfer forces developed in the device without failure, granting the ability to support gravity loads even after strong seismic events. Without a proper design procedure backend on the proposed parameters values, the design process may lead to oversized connection systems, resulting in significantly higher construction costs.

The black continuous line represents the algebraic solution for the bearing force F_{lim} correspondng to a limit displacement d_{lim} (see Table 2). Values recorded by the OpenSEES software

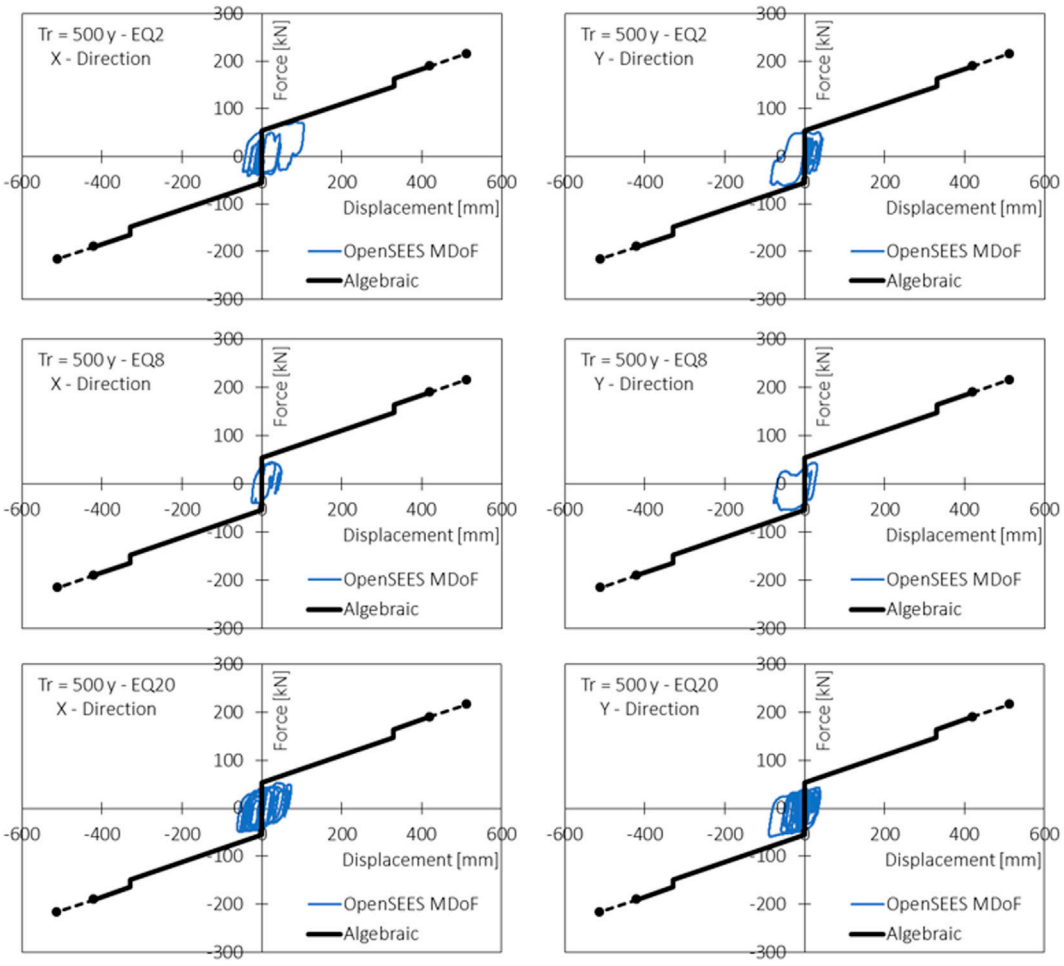

FIGURE 11
Single DCCSS bearing force vs. displacement relationship in *X* and *Y* directions for three example earthquakes (EQ2; EQ8; EQ20 for a return p oferiod 500 years.

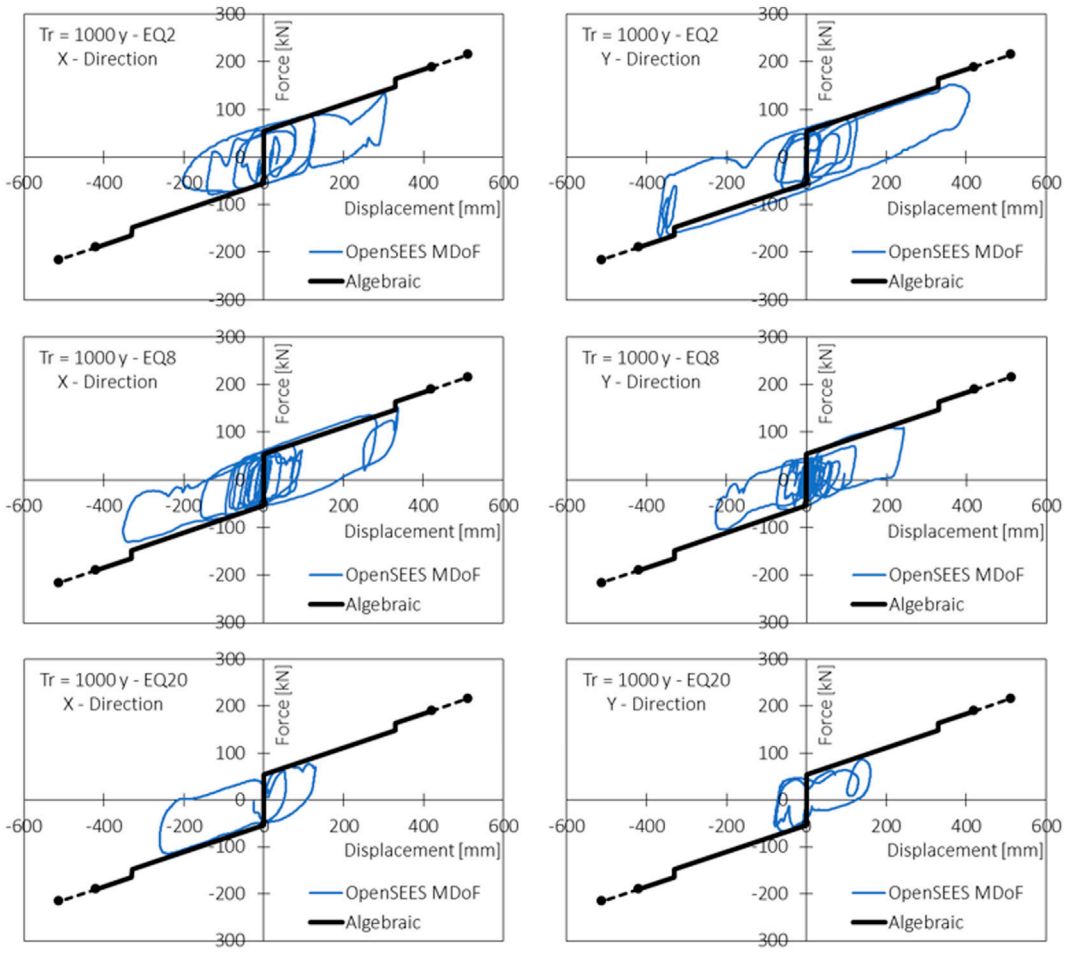

FIGURE 12
Single DCCSS bearing force vs. displacement relationship in *X* and *Y* directions for three example earthquakes (EQ2; EQ8; EQ20 for a return period of 1,000 years.

ranged around the F_{lim} algebraic force with some deviation due to the friction coefficient dependency on the axial force and instantaneous velocity variabilities. Among the 16 cases that reached d_{lim} (one for $T_R = 1000y$ and 15 for $T_R = 2500y$), the recorded values of F_{lim} were as follows: minimum 118.88 kN, mean 172,83 kN, and maximum 215.79 kN. Only three cases out of 16 showed a value of force higher than that predicted by the algebraic solution, resulting in a 19% probability of a non-conservative solution.

More detailed insight into the results of the analyses are provided in Figures 11–13, which shows the comparison between the algebraic solution and the MDoF model forces vs. displacement behaviour of a DCCSS bearing located in the central position, taking into account three example earthquakes for each return period (EQ2, EQ8, and EQ20 (indicated in Figure 10.

Intensities corresponding to the design force (CLS, $T_R = 1000y$), characterized by a few cases of over-stroke displacement, stand out as those best fitted by the proposed analytical formulation (Figure 11). Figures 11, 12 show the differences between the MDoF model and the Regime I algebraic solution proposed by basic theories about seismic intensities lower or equal to those featured in simulations.

Some differences between the numerical and algebraic results can be observed for high seismic intensities ($T_R = 2500y$) when the over-stroke is activated (Figure 13), and are linked to the axial force and the strong influence of the velocity variabilities on the shape of the force-displacement law. For the case study, results show a good approximation of the frictional shear force estimation provided by the algebraic solution.

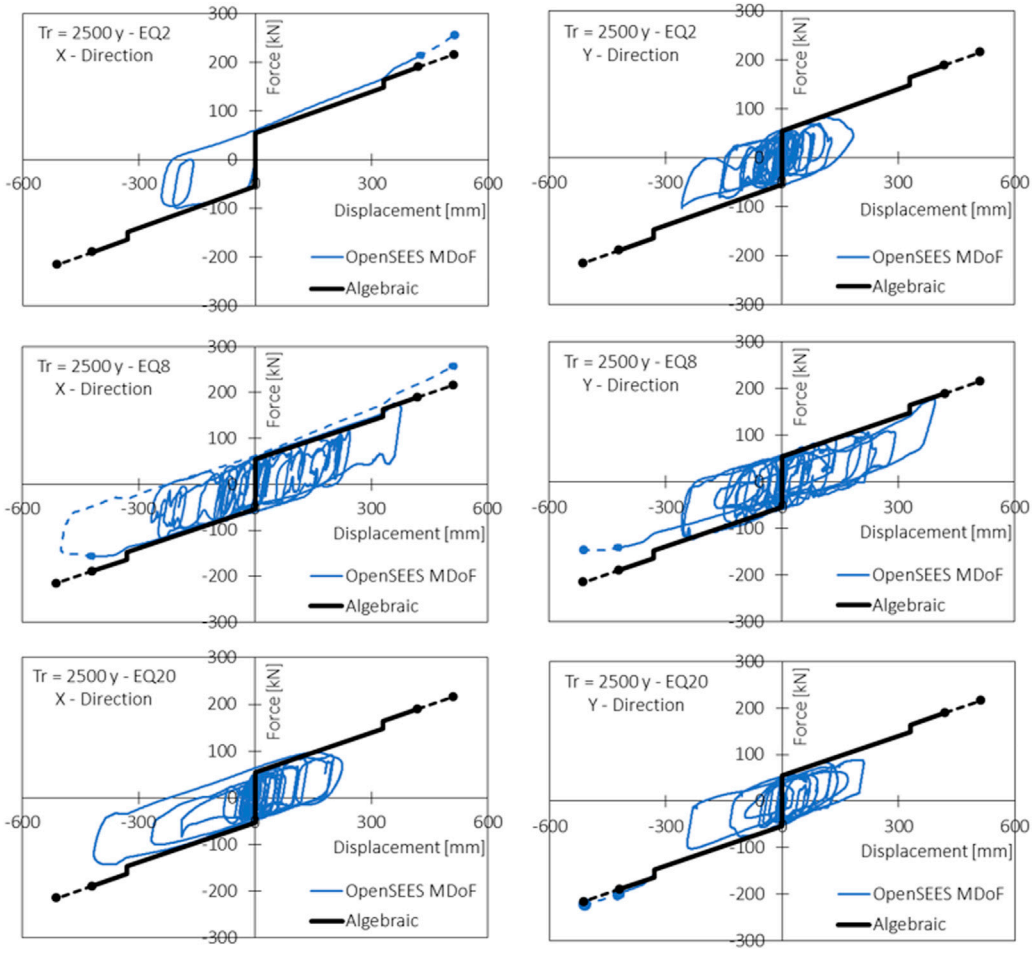

FIGURE 13
Single DCCSS bearing force vs. displacement relationship in *X* and *Y* directions for three example earthquakes (EQ2; EQ8; EQ20 for a return period of 2,500 years.

4 Conclusion

Starting with the formulations of past theories, this paper presents an extension of the DCCSS bearing force-displacement relationship to describe over-stroke behaviour in the simplified case of a DCCSS with an equal radii of curvature and equal friction coefficients for both concave plates.

The proposed algebraic solution is capable of representing forces that act on the isolation device for displacements higher than the geometric housing plate capacity, and is capable of identifying the displacements that correspond with the attainment of real limit conditions.

The proposed formulation has been provided to describe the sloping dog bone shape constitutive law estimated through experimental tests of the over-stroke regime when the rigid slider of the DCCSS bearing runs on the edge of the housing plates, exceeding its geometric capacity displacement. The algebraic solution for two failure mechanisms, which accounts for the rigid slider overturning kinematic and maximum contact pressure on the sliding interface, has been provided in terms of algebraic equations for the force-displacement relationships. The solution is valid for DCCSS bearings with a rigid slider and flat rim, equal radii of curvature, and friction coefficients on both of the concave plates.

The utility of the proposed solution is in checking the validity of numerical solutions of more complex models, and in designing the actual limit displacement and maximum shear force of the device with high accuracy. Furthermore, the maximum shear force F_{lim} algebraic expression provided is of crucial importance to the design of the connections between the isolation devices and structure.

To validate the application of the proposed solution, non-linear dynamic analyses were implemented in OpenSees software to represent the case study of a six-storey RC frame building seismically isolated at the ground level with DCCSS bearings with over-stroke capacity. A three-dimensional MDoF model of the

superstructure was upgraded with base isolation, implementing a multivariable friction model for the over-stroke displacement of DCCSS bearings, which also accounts for the effects of velocity and axial load variabilities. Additionally, structural analyses at intensity levels around design one have been carried out.

The results obtained by non-linear analysis strongly concurred with the results from the direct implementation of the proposed algebraic equations derived from the static condition. In particular, the proposed algebraic solution very accurately represented the shear forces acting on the single DCCSS bearing in the over-stroke regime. Furthermore, the results showed how the high accelerogram variability significantly affects the structural response. The proposed algebraic solution accounting for the over-stroke behaviour of DCCSS isolators should provide a safer tool for designers.

Further research should be carried out on the topic, and additional experimental testing campaigns are needed to evaluate possible dependencies of the over-stroke effect of DCCSS devices. The findings could help to facilitate highly accurate estimations of the seismic risk of seismically isolated structures with slider bearings, and develop appropriate safety factors in future building codes.

Data availability statement

The data analyzed in this study is subject to the following licenses/restrictions: The datasets analysed during the current study are available from the corresponding author on reasonable request. Requests to access these datasets should be directed to antonio.dicesare@unibas.it.

Author contributions

All authors contributed to the study conception and design. Material preparation, data collection, and analyses were performed by AD and AT. The first draft of the manuscript was written by AD and AT, and all authors read and approved the submitted manuscript.

Funding

This work was supported by RELUIS 2022–2024 project funded by the Italian Civil Protection Department.

Acknowledgments

The authors would like to acknowledge the financial support from the RELUIS 2022–2024 project WP 15, funded by the Italian Civil Protection Department, and FIP MEC srl (https://www.fipmec.it/) for providing support during the laboratory testing phase.

Conflict of interest

The authors declare that the research was conducted in the absence of any commercial or financial relationships that could be construed as a potential conflict of interest.

The reviewer MF declared a past co-authorship with the authors AC, FP to the handling editor.

Publisher's note

References

Almazán, J. L., and De La Llera, J. C. (2011). Analytical model of structures with frictional pendulum isolators. *Earthq. Eng. Struct. Dyn.* 31, 305–332.

Almazán, J. L., De La Llera, J. C., and Inaudi, J. A. (1998). Modelling aspects of structures isolated with the friction pendulum system. *Earthq. Eng. Struct. Dyn.* 27, 845–867.

Bao, Y., Becker, T. C., and Hamaguchi, H. (2017). Failure of double friction pendulum bearings under pulse-type motions. *Earthq. Eng. Struct. Dyn.* 46 (5), 715. doi:10.1002/eqe.2827

Becker, T. C., and Mahin, S. A. (2012). Correct treatment of rotation of sliding surfaces in a kinematic model of the triple friction pendulum bearing. *Earthq. Engng. Struct. Dyn.* 42, 311–317. doi:10.1002/eqe.2199

Becker, T. C., and Mahin, S. A. (2012). Experimental and analytical study of the Bi-directional behavior of the triple friction pendulum isolator. *Earthq. Eng. Struct. Dyn.* 41, 355–373. doi:10.1002/eqe.1133

Belfiore, N. P., Di Benedetto, A., and Pennestrì, E. (2000). *Foundations of mechanics applied to machines*. Milano, Italy: Casa Editrice Ambrosiana, 153–194. In Italian.

Bianco, V., Monti, G., and Belfiore, N. P. (2020). Fine-tuning of modelling strategy to simulate thermo-mechanical behavior of double friction pendulum seismic isolators. *Ned. Univ. J. Res.* 3, 165–172. doi:10.35453/NEDJR-STMECH-2019-0058

Bianco, V., Monti, G., Belfiore, N. P., and Vailati, M. (2021). Multibody kinematics of the double concave curved surface sliders: From supposed compliant sliding to suspected stick-slip. *Pract. Period. Struct. Des. Constr.* 26 (3), 04021024. doi:10.1061/(asce)sc.1943-5576.0000581

Cardone, D., Viggiani, L. R. S., Perrone, G., Telesca, A., Di Cesare, A., Ponzo, F. C., et al. (2022). Modelling and seismic response analysis of existing Italian residential RC buildings retrofitted by seismic isolation. *J. Earthq. Eng.*, 1–25. doi:10.1080/13632469.2022.2036271

Constantinou, M. C., Mokha, A., and Reinhorn, A. (1990). Teflon bearings in base isolation, II: Modeling. *J. Struct. Eng. (N. Y. N. Y).* 116, 455–474. doi:10.1061/(asce)0733-9445(1990)116:2(455)

De Domenico, D., Ricciardi, G., and Benzoni, G. (2018). Analytical and finite element investigation on the thermo-mechanical coupled response of friction isolators under bidirectional excitation. *Soil Dyn. Earthq. Eng.* 106, 131–147. doi:10.1016/j.soildyn.2017.12.019

De Domenico, D., Ricciardi, G., Infanti, S., and Benzoni, G. (2019). Frictional heating in double curved surface sliders and its effects on the hysteretic behavior: An experimental study. *Front. Built Environ.* 5. doi:10.3389/fbuil.2019.00074

Decanini, L. D., Liberatore, L., and Mollaioli, F. (2014). Strength and stiffness reduction factors for infilled frames with openings. *Earthq. Eng. Eng. Vib.* 13, 437–454. doi:10.1007/s11803-014-0254-9

Decreto Ministreriale (1986). *Norme Tecniche relative alle costruzioni sismiche, Decreto ministeriale del 24 gennaio 1986*. Rome, Italy: Ministero delle Infrastrutture e dei Trasporti.

Di Cesare, A., Ponzo, F. C., and Telesca, A. (2021). Improving the earthquake resilience of isolated buildings with double concave curved surface sliders. *Eng. Struct.* 228 (111498), 111498. ISSN 0141-0296. doi:10.1016/j.engstruct.2020.111498

Di Cesare, A., Ponzo, F. C., Telesca, A., Nigro, D., Castellano, G., Infanti, S., et al. (2019). *Modelling of the over stroke displacement of curved surface sliders using OpenSEES*. Hong Kong: OpenSEES Days Eurasia.

Fenz, D. M., and Constantinou, M. C. (2006). Behaviour of the double concave Friction Pendulum bearing. *Earthq. Eng. Struct. Dyn.* 35, 1403–1424. doi:10.1002/eqe.589

Fenz, D. M., and Constantinou, M. C. (2008). *Report No. MCEER-08-0007*. Buffalo, NY: Multidisciplinary Center for Earthquake Engineering Research.Mechanical behavior of multi-spherical sliding bearings

Fenz, D. M., and Constantinou, M. C. (2008). Spherical sliding isolation bearings with adaptive behavior: Experimental verification. *Earthq. Eng. Struct. Dyn.* 37, 185–205. doi:10.1002/eqe.750

Furinghetti, M., Lanese, I., and Pavese, A. (2020). Experimental assessment of the seismic response of a base-isolated building through a hybrid simulation technique. *Front. Built Environ.* 6. doi:10.3389/fbuil.2020.00033

Furinghetti, M., and Pavese, A. (2021b) Modeling strategies for the lateral response of curved surface slider devices under extreme displacement demands. Proceedings of the COMPDYN 2021, 8th ECCOMAS Thematic Conference on Computational Methods in Structural Dynamics and Earthquake Engineering, June 2021, Streamed from Athens, Greece.

Furinghetti, M., Yang, T., Calvi, P. M., and Pavese, A. (2021a). Experimental evaluation of extra-stroke displacement capacity for Curved Surface Slider devices. *Soil Dyn. Earthq. Eng.* 146, 106752. doi:10.1016/j.soildyn.2021.106752

Ibarra, L. F., Medina, R. A., and Krawinkler, H. (2005). Hysteretic models that incorporate strength and stiffness deterioration. *Earthq. Eng. Struct. Dyn.* 34, 1489–1511. doi:10.1002/eqe.495

Iervolino, I., Chioccarelli, E., and Convertito, V. (2011). Engineering design earthquakes from multimodal hazard disaggregation. *Soil Dyn. Earthq. Eng.* 31, 1212–1231. doi:10.1016/j.soildyn.2011.05.001

Iervolino, I., Spillatura, A., and Bazzurro, P. (2019) RINTC-E project: Towards the assessment of the seismic risk of existing buildings in Italy. Proceedings of the 7th International conference on computational methods in structural dynamics and earthquake engineering – COMPDYN 2019, June 2019, Crete, Greece.

Iervolino, I., Spillatura, A., and Bazzurro, P. (2018). Seismic reliability of code-conforming Italian buildings. *J. Earthq. Eng.* 22 (2), 5–27. doi:10.1080/13632469.2018.1540372

Lomiento, G., Bonessio, N., and Benzoni, G. (2013). Friction model for sliding bearings under seismic excitation. *J. Earthq. Eng.* 17, 1162–1191. doi:10.1080/13632469.2013.814611

Mazza, F., Mazza, M., and Vulcano, A. (2017). Nonlinear response of rc framed buildings retrofitted by different base-isolation systems under horizontal and vertical components of near-fault earthquakes. *Earthquakes Struct.* 12 (1), 135–144. doi:10.12989/eas.2017.12.1.135

Mckenna, F., Fenves, G. L., Scott, M. H., and Jeremic, B. (2000). *Open system for earthquake engineering simulation (OpenSEES)*. Berkeley (CA): PEER Center, University of California.

Mostaghel, N., and Davis, T. (1997). Representations of Coulomb friction for dynamic analysis. *Earthq. Eng. Struct. Dyn.* 26 (5), 541–548. doi:10.1002/(sici)1096-9845(199705)26:5<541::aid-eqe660>3.0.co;2-w

Nikravesh, P. E. (2018). *Planar multibody dynamics-formulation, programming with , and applications*. New York, NY, USA: CRC Press, Taylor & Francis Group, 355–382.

NTC (2018). *Norme Tecniche per le Costruzioni, Decreto ministeriale del 17 gennaio 2018*. Rome, Italy: Ministero delle Infrastrutture e dei Trasporti.

Pavese, A., Furinghetti, M., and Casarotti, C. (2018). Experimental assessment of the cyclic response of friction-based isolators under bidirectional motions. *Soil Dyn. Earthq. Eng.* 114, 1–11. doi:10.1016/j.soildyn.2018.06.031

Pigouni, E. A., Castellano, M. G., Infanti, S., and Colato, G. P. (2019). Full-scale dynamic testing of pendulum isolators (Curved surface sliders). *Soil Dyn. Earthq. Eng.* 130, 105983. doi:10.1016/j.soildyn.2019.105983

Ponzo, F. C., Di Cesare, A., Telesca, A., Nigro, D., Castellano, M. G., and Infanti, S. (2020) Influence of DCCSS Bearings Over-Stroke and breakaway on the seismic response of isolated buildings. Proceedings of the 17th World Conference on Earthquake Engineering, September 2020, Sendai, Japan.

Ponzo, F. C., Di Cesare, A., Telesca, A., Pavese, A., and Furinghetti, M. (2021) Advanced modelling and risk analysis of RC buildings with sliding isolation systems designed by the Italian seismic code. *Appl. Sci. (Basel).*, 11, 1938, doi:10.3390/app11041938

Ponzo, F. C., Di Cesare, A., Leccese, G., and Nigro, D. (2017). Shake table testing on restoring capability of double concave friction pendulum seismic isolation systems. *Earthq. Eng. Struct. Dyn.* 46, 2337–2353. doi:10.1002/eqe.2907

Ponzo, F. C., Di Cesare, A., Leccese, G., and Nigro, D. (2019). Standard requirements for the recentering capability of curved surface sliders. *Ing. Sismica* 36, 95–106.

Popov, V. (2010). *Contact mechanics and friction-physical principles and applications*. Berlin, Germany: Springer, 175–230.

Quaglini, V., Dubini, P., and Poggi, C. (2012) Experimental assessment of sliding materials for seismic isolation systems. *Bull. Earthq. Eng.*, 10, 717, doi:10.1007/s10518-011-9308-9

Quaglini, V., Gandelli, E., and Dubini, P. (2019). Numerical investigation of curved surface sliders under bidirectional orbits. *Ing. Sismica* 36, 118–136.

Ricci, P., Manfredi, V., Noto, F., Terrenzi, M., Petrone, C., Celano, F., et al. (2018). Modeling and seismic response analysis of Italian code-conforming reinforced concrete buildings. *J. Earthq. Eng.* 22, 105–139. doi:10.1080/13632469.2018.1527733

Sarlis, A. A., and Constantinou, M. C. (2016). A model of triple friction pendulum bearing for general geometric and frictional parameters. *Earthq. Eng. Struct. Dyn.* 45, 1837–1853. doi:10.1002/eqe.2738

Sarlis, A. A., and Constantinou, M. C. (2013). "Model of triple friction pendulum bearing for general geometric and frictional parameters and for uplift conditions," *Report No. MCEER-13-0010* (Buffalo, NY: Multidisciplinary Center for Earthquake Engineering Research).

Shabana, A. A. (2001). *Computational dynamics*. New York, NY, USA: John Wiley & Sons, 295–378.

Tsai, C. S., Chiang, T. C., and Chen, B. J. (2005). Experimental evaluation of piecewise exact solution for predicting seismic responses of spherical sliding type isolated structures. *Earthq. Eng. Struct. Dyn.* 34 (9), 1027–1046. doi:10.1002/eqe.430

Zayas, V. A., Low, S. S., and Mahin, S. A. (1987). *The FPS earthquake resisting system; report No. 87-01*. Berkley, CA, USA: Earthquake Engineering Research Center.